Supplement of The Cryosphere, 19, 3849–3872, 2025
https://doi.org/10.5194/tc-19-3849-2025-supplement

The Cryosphere Open Access EGU

Supplement of

Sub-shelf melt pattern and ice sheet mass loss governed by meltwater flow below ice shelves

Franka Jesse et al.

Correspondence to: Franka Jesse (t.f.jesse@uu.nl)

High-melt scenario fields

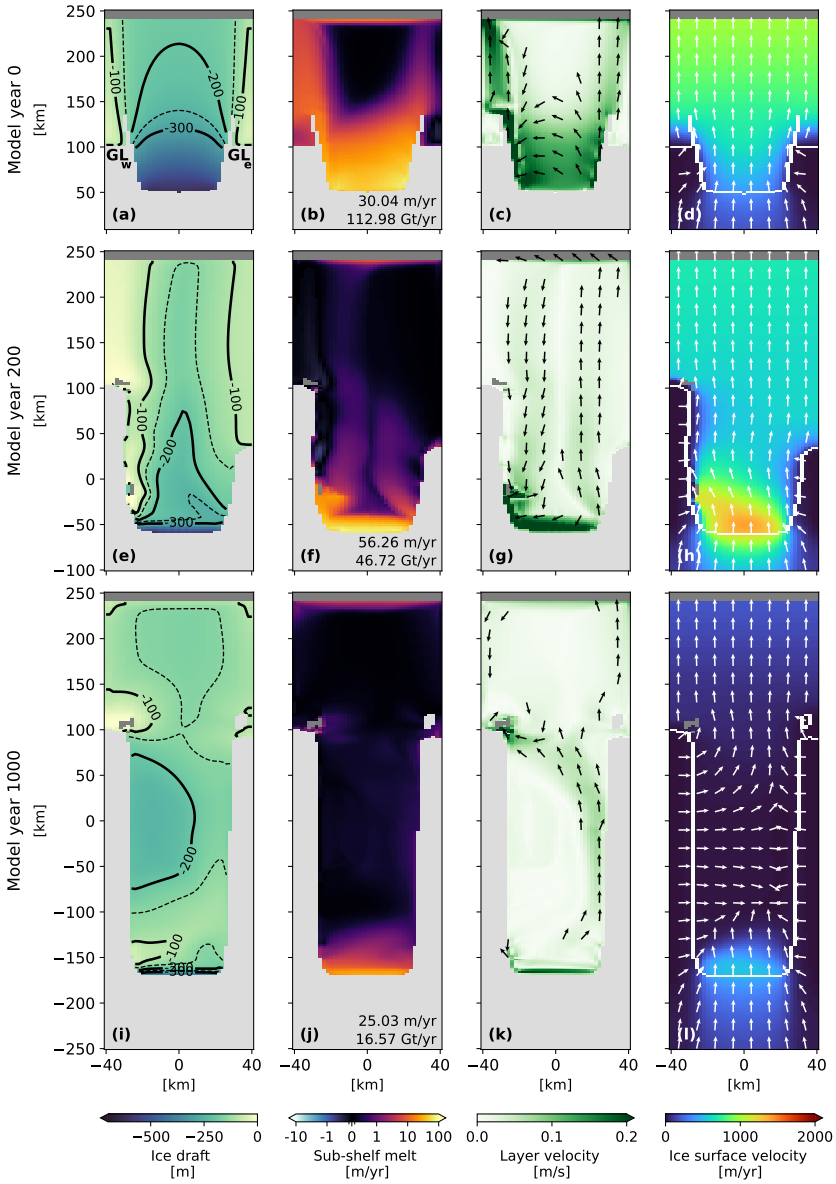

Figure S1: Same as Fig. 4, but now for high-melt scenario LADDIE experiment (LA_H). An animation of this figure, showing time slices every 10 model years, is provided in the video supplements.

As indicated in Sect. 3.1, the LADDIE experiments show a similar transient response in the high-melt scenario (LA_H) relative to the moderate-melt scenario (LA_M). One big difference is the duration of the phase of peak volume loss (Fig. 7a, b), which we find to be shorter in the high-melt scenario due to the negative feedback between melt-through and western margin melt. This negative feedback shows from the LA_H melt pattern and meltwater layer velocities in model year 200 (Fig. S1f, g). It shows the western boundary current cannot continue further along the western margin when it encounters one of the areas of melt-through in the ice shelf. Moreover, the eastward shift of the channelised meltwater flow occurs earlier in the high-melt scenario, allowing the channel to migrate fully to the east by the end of the simulation (Fig. S1k). Similar to the LA_M experiment, this channel is associated with low melt rates.

The parameterised experiment under the high-melt forcing scenario show a similar feedback between melt and geometry as seen under the moderate-melt forcing scenario (Fig. S2). Here, we highlight the main differences for each of the parameterisations. For the Quadratic parameterisation, in the high-melt experiment, melt rates remain to strong to facilitate pinning on the margins at the end of the simulation (Fig. S2j,k), unlike in the moderate-melt experiment (Fig. 6j,k). The absence of pinning results in weaker buttressing which leads to slightly higher final ice velocities at the end of the high-melt

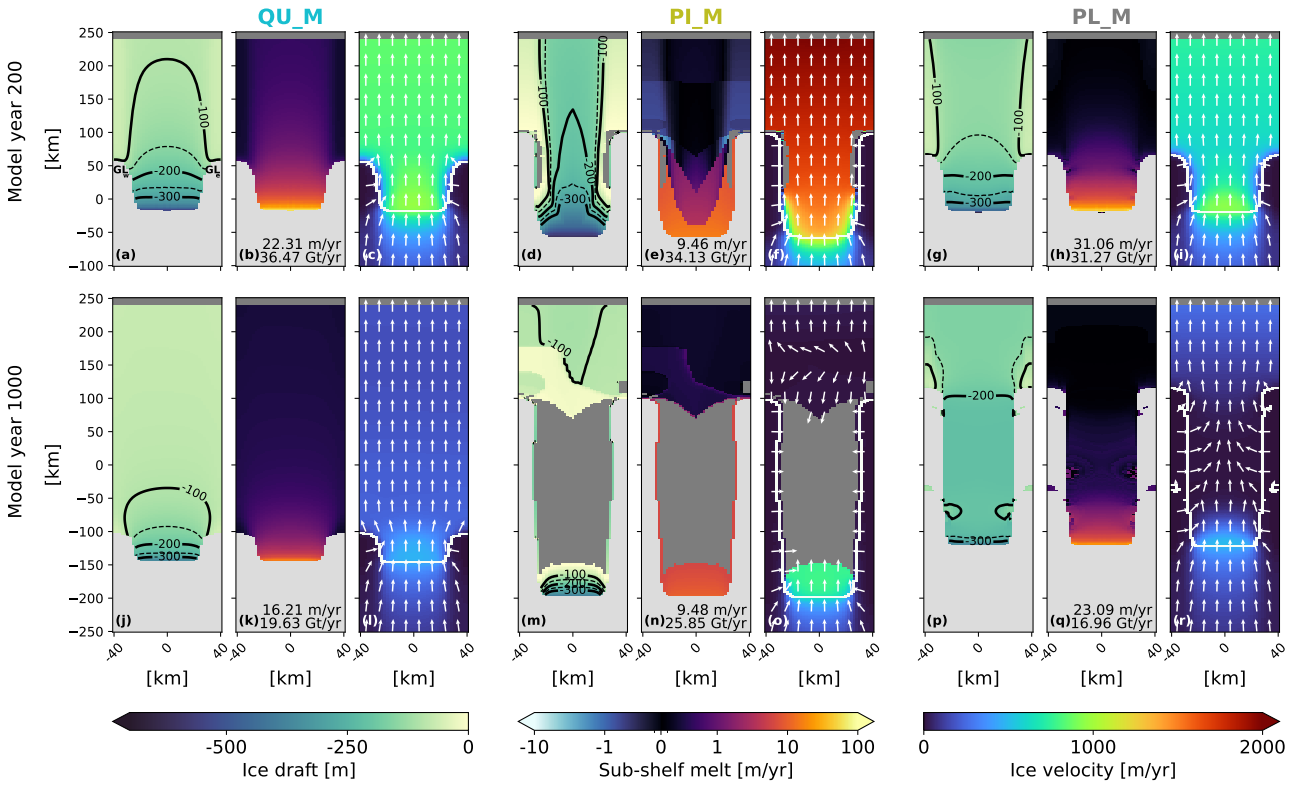

Figure S2: Same as Fig. 6, but now for the high-melt scenario Quadratic, PICO, and Plume experiments (QU_H, PI_H, PL_H). An animation of this figure, showing time slices every 10 model years, is provided in the video supplements.

experiment (Fig. S2l). For the PICO parameterisation, the high-melt scenario induces a wider melt-through of the ice shelf (Fig. S2d), causing strong dynamical detachment, leading to higher ice velocities than the moderate-melt scenario after 200 years (Fig. S2f). Over longer timescales, enhanced melt rates lead to the near-complete loss of ice within the margins (Fig. S2m). Consequently, ice velocities at the grounding line remain relatively high compared to the PI_M experiment (Fig. S2o). For the Plume parameterisation, the primary difference lies in the timing of margin pinning and readvance, which occur later in the high-melt scenario compared to the moderate-melt scenario. This delay leads to a more retreated central grounding line by the end of the simulation (Fig. S2r).

Central cross-section of the ice geometry

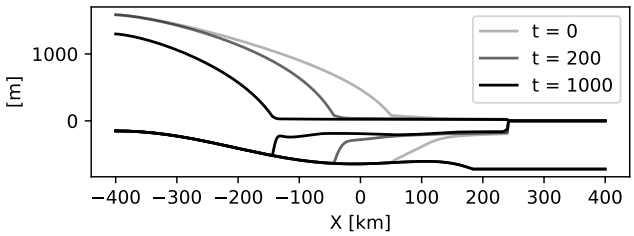

Figure S3: Central cross-section (Y = 0 km) of the ice geometry of the LA_M experiment. The surface height and ice shelf draft are shown for three time slices (identical to the time slices shown in Fig. 4). The bottom line shows the bed geometry.

For the LA_M experiment, the two-dimensional draft plots in Fig. 4 reveal a pronounced ice thickness gradient across the grounding line after 200 and 1000 years (Fig. 4e, i). To better illustrate this gradient, Fig. S3 presents a central cross-section of the ice surface elevation, ice draft, and underlying bathymetry at the start of the experiment, as well as after 200 and 1000 years. This figure highlights the progressive steepening of the draft near the grounding line over time, especially by the end of the simulation. As noted in the discussion, a different sliding law may not support this steep gradient, potentially leading to a slightly altered feedback between melting and ice geometry.

Calving impact

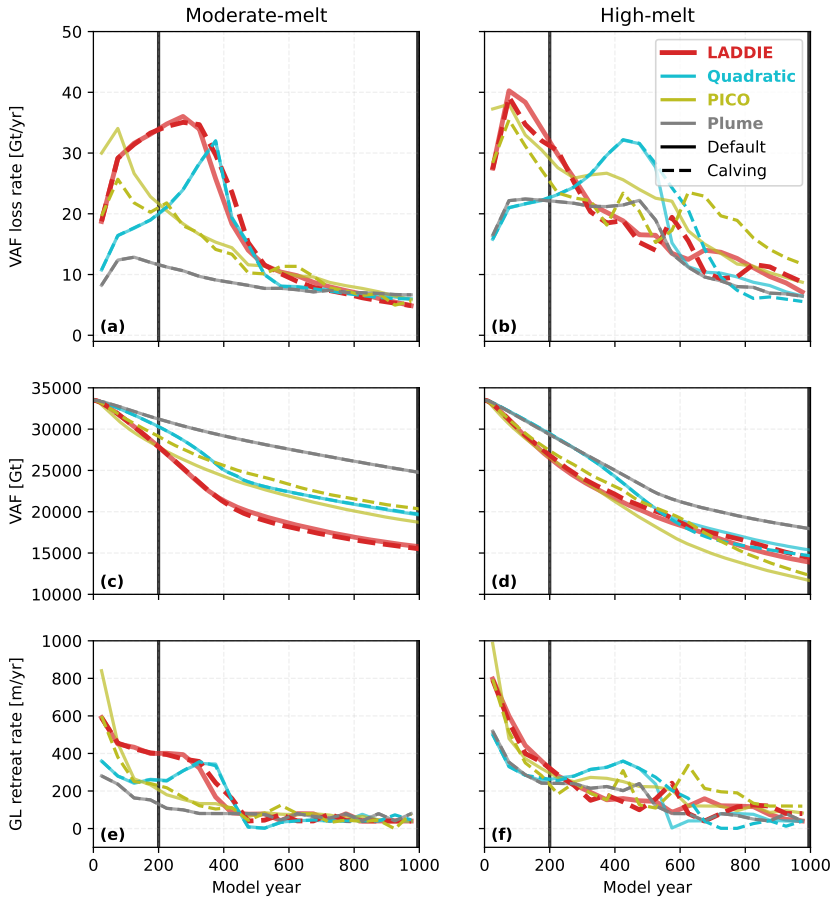

Figure S4: Same as Fig. 7, but now the dashed lines represent the simulations with calving applied using a threshold thickness of 100 meters. The video supplements include animations for these simulations.

To test the sensitivity to calving, all experiments were repeated with a calving threshold of 100 meters (i.e., floating ice is removed when thinner than 100 meters). For LADDIE, and the Quadratic and Plume parameterisation, applying a calving threshold has minimal impact on the transient behaviour (Fig. S4). The PICO experiments show a larger impact of calving, primarily in the high-melt scenario, with volume loss rates revealing an earlier dip (years 200 to 600), but then a later peak compared to the default experiments (years 600 to 800) (Fig. S4b). The stronger influence of calving in PICO is explained by the calving front retreat modifying the ice shelf-wide box structure and melt pattern. For LADDIE, Quadratic and Plume, calving front retreat does not affect melting closer to the grounding line. Animations of the horizontal fields of ice draft, sub-shelf melt, ice surface velocity and, for LADDIE, layer velocity are provided in the video supplements.

Retuning experiments

Table S1 shows the values of the tuning parameters for the default tuning scenario based on the moderate-melt scenario (same as Table 2), and for the retuned experiments, where we retuned the parameterisations to match deep melt rates with LADDIE in the high-melt scenario. For PICO, the overturning coefficient C is kept constant over the two tuning scenarios.

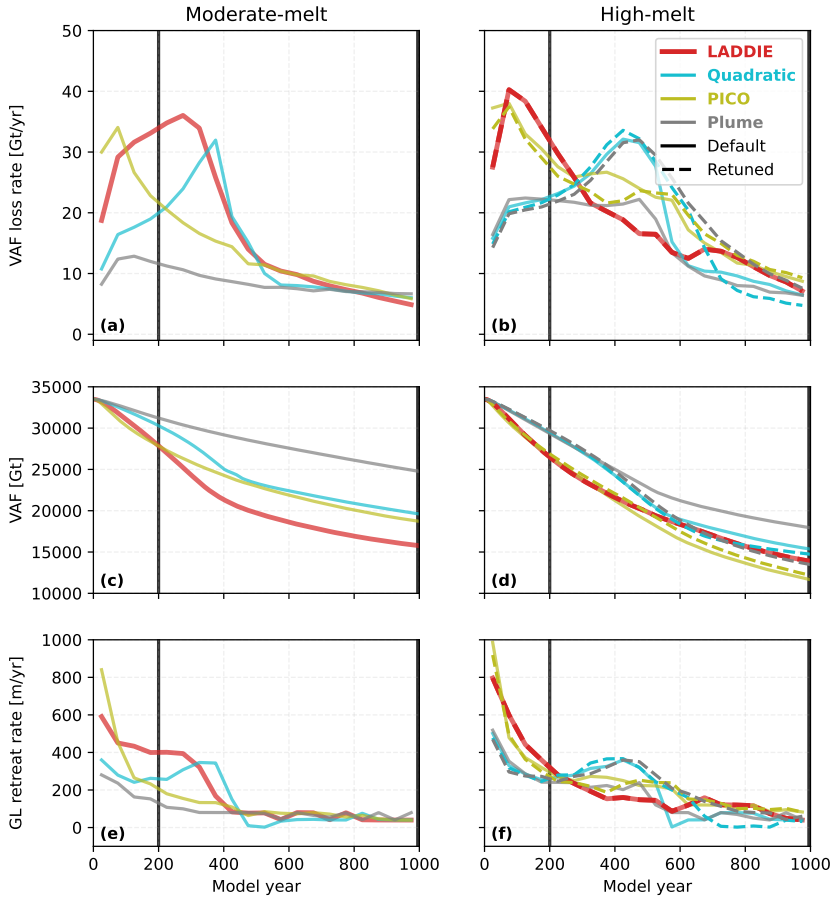

Figure S5: Same as Fig. 7, but now the dashed lines represent the simulations with melt rates retuned to match deep melt rate in high-melt scenario.

For all parameterisations, retuning leads to lower integrated melt rates and deep melt rates at the start of the simulation. For all parameterisations, retuning does not have a big effect on the transient behaviour over the first 200 years (Fig. S5). For the Quadratic and PICO parameterisations, retuning does not lead to major differences in transient VAF loss and grounding line retreat compared to the default tuning (Fig. S5b, g). This also leads to relatively similar VAF over time (Fig. S5d). For the Plume parameterisation, retuning to match deep average melt rates enables peak VAF loss rates to increase substantially compared to the default run, leading to stronger VAF loss and a substantial lower resulting VAF at the end of the simulation (Fig. S5d). The retuned run does not readvance on the lateral margins, whereas the default run does around model year

Table S1: Tuning parameter values for the different sub-shelf melt implementations. Default tuning refers to the tuning used for the main experiments presented in this study, with average deep melt rates of 16.75 $\pm$ 1.00 m/yr under the moderate-melt scenario. High-melt retuning refers to the tuning used for our retuning sensitivity tests, with average deep melt rates of 30.00 $\pm$ 1.00 m/yr under the high-melt scenario.

Sub-shelf melt option	default mod-melt tuning γ_T [ms^{-1}]	high-melt retuning γ_T [ms^{-1}]	Overturning coefficient C [m^3 kg^{-1}]
LADDIE	1.47×10^{-4}	1.47×10^{-4}	
Quadratic	14.16×10^{-4}	12.56×10^{-4}	
PICO	1.28×10^{-4}	0.93×10^{-4}	0.23×10^{-6}
Plume	16.87×10^{-4}	5.69×10^{-4}	

500. We suggest that this difference arises from the tuning affecting the length scale at which melt transitions to refreezing (Appendix A3). This length scale is shorter for the default run, allowing refreezing closer to the grounding line, consequently allowing for repinning. Animations of the horizontal fields of ice draft, sub-shelf melt, ice surface velocity and, for LADDIE, layer velocity are provided in the video supplements.

Computational cost comparison

Computational costs are shown in Table S2. For the LADDIE experiments, IMUA-ICE runs on 31 cores, and LADDIE runs on 1 core. For the parameterised experiments, IMAU-ICE uses 32 cores. IMAU-ICE uses an iterative solver for the velocity fields, hence when geometries are more complex (e.g. pinning points), simulations can take longer. The simulations were run on an HPC with cores with variable efficiency.

Table S2: Overview on the computational cost of the perturbation experiments. Real time refers to the duration of a 1000-year simulation on one node with 32 cores.

Experiment	Real time	CPU hours
LA_M	75 hours	2400
LA_H	72 hours	2304
QU_M	8 hours	256
QU_H	24 hours	768
PI_M	9 hours	288
PI_H	11 hours	352
PL_M	8 hours	256
PL_H	9 hours	288